



A parametric study of a flexible ocean tower

S.N. Kuchnicki *, H. Benaroya

Department of Mechanical and Aerospace Engineering, Rutgers University, 98 Brett Road, Piscataway, NJ 08854, USA

Abstract

Offshore compliant structures are a valuable and attractive option for conditions involving operation in deep water because of their reduced structural weight. One class of offshore compliant structure is the articulated tower, which does not use guylines or tethers to provide a restoring force; rather, the articulated tower relies on a large buoyancy moment to maintain its orientation. This paper examines a continuous, elastic model of an articulated tower undergoing planar motion. Forces due to gravity, buoyancy, and waves are considered, and the nonlinear governing equations of motion derived using Hamilton's Principle. These equations of motion are discretized using the finite difference method, and solved numerically. A proposed simplification of the derived elastic equations is presented, and the simplified model is shown to provide a good upper bound on the motion and a good picture of the qualitative behavior. A parameter study on the tower system is performed, demonstrating the stability of the tower system in the presence of different environmental loads and under different tower configurations. © 2002 Elsevier Science Ltd. All rights reserved.

1. Introduction

Compliant platforms such as articulated towers are attractive alternatives for many deep-water applications due to their reduced structural weight as compared to traditional platforms. The tower does not resist forces due to wind, waves, and currents; rather, these forces are countered via a large buoyancy force and/or a set of guylines. Due to the nature of the loads experienced by the tower, an examination of the tower behavior taking the elastic motion of the structure into account is required. An overview of several compliant platform types and their applications is given by Adrezin et al. [1]. A schematic of the tower system is given in Fig. 1.

2. Equations of motion

To arrive at the equations of motion for the flexible tower system, we apply Hamilton's Principle under the following assumptions:

- The tower is an inextensible beam moving only in the x, y plane; i.e., $y = y(x, t)$.
- The tower is flexible, having bending rigidity EI .
- Longitudinal vibrations are negligible in comparison to rotational and lateral vibrations.
- The tower length is much greater than its diameter ($L \gg D$).
- The tower is a slender, smooth structure having constant radius.
- For this study, the top mass is zero, and we consider only wave loads on the tower, ignoring wind and wave slamming forces.
- The tower is hollow, with outer diameter D_o and inner diameter D_i .

* Corresponding author.

E-mail addresses: kuchnick@rci.rutgers.edu (S.N. Kuchnicki), benaroya@rci.rutgers.edu (H. Benaroya).

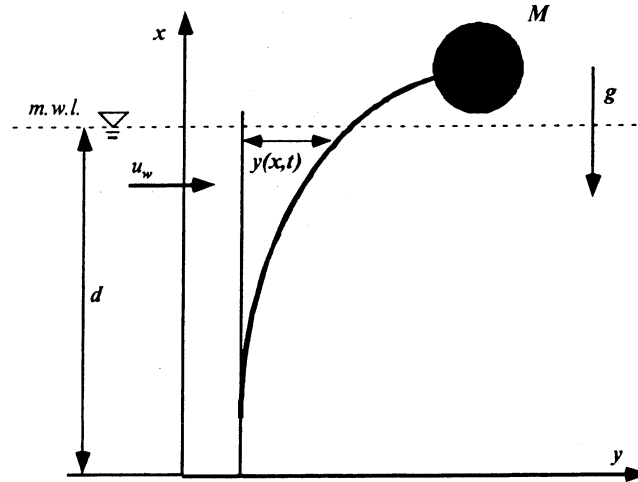


Fig. 1. Schematic of the flexible tower system.

Table 1
Definition of symbols

Symbol	Meaning
ρ_T, ρ	Densities of tower and of water, respectively
D_o, D_i	Tower outer and inner diameter, respectively
L	Tower length
E	Tower Young's modulus
d	Mean water level
C_M, C_D, C_A	Coefficients of inertia, drag, and added mass, respectively
u_w, w_w	Wave velocity in horizontal (y) and vertical (x) directions
y_i	Derivative of y with respect to variable i

The general form of the Euler–Lagrange equations for this system is [5]

$$\frac{\partial \mathcal{L}}{\partial y} - \frac{\partial}{\partial t} \left(\frac{\partial \mathcal{L}}{\partial y_t} \right) - \frac{\partial}{\partial x} \left(\frac{\partial \mathcal{L}}{\partial y_x} \right) + \frac{\partial^2}{\partial x^2} \left(\frac{\partial \mathcal{L}}{\partial y_{xx}} \right) + \frac{\partial^2}{\partial x \partial t} \left(\frac{\partial \mathcal{L}}{\partial y_{xt}} \right) = Q, \quad (1)$$

where y_i refers to differentiation of variable y with respect to variable i , Q is the generalized force, and the Lagrangian \mathcal{L} is taken as $\mathcal{L} = \mathbf{K}_E - \mathbf{P}_E$, where \mathbf{K}_E is the kinetic energy of the system, and \mathbf{P}_E is the potential energy. Note that we assume no external damping, only internal structural damping. In preparation for the sections that follow, Table 1 summarizes the symbols that will be used for different physical quantities in the derivations.

2.1. Kinetic energy

For this system, the kinetic energy will consist of two components, one due to the rectilinear velocity of the tower, and the other caused by the tower angular velocity. Using a method like that in [2], we find the rectilinear kinetic energy to be

$$\mathbf{K}_E^L = \int_0^L \frac{1}{8} \pi [\rho_T (D_o^2 - D_i^2) + C_A \rho D_o^2] y_t^2 dx. \quad (2)$$

Note that the tower end mass is taken to be zero for this study. The angular kinetic energy is then:

$$\mathbf{K}_E^A = \int_0^L \frac{1}{128} \pi [\rho_T (D_o^4 - D_i^4) + C_A \rho D_o^4] \frac{y_{xt}^2}{(1 + y_x^2)^2} dx. \quad (3)$$

Since the system is submerged in a fluid, the added mass effects of the fluid are accounted for through the added mass coefficient.

2.2. Potential energy

The potential energy of this system is due to two sources: bending strain and the applied loading due to gravity and buoyancy. The bending strain energy may be expressed as

$$\mathbf{P}_E^B = \int_0^L \frac{1}{128} \pi E (D_o^4 - D_i^4) \frac{y_{xx}^2}{(1 + y_x^2)^3} \sqrt{1 + y_x^2} dx, \quad (4)$$

and the potential energy due to gravity and buoyancy forces is

$$\mathbf{P}_E^G = \int_0^L \left\{ \frac{1}{4} \pi \rho g D_o^2 (l_s - \bar{x}) (\sqrt{1 + y_x^2} - 1) - \left[\frac{1}{4} \pi \rho_T (D_o^2 - D_i^2) (l - \bar{x}) + M \right] g (\sqrt{1 + y_x^2} - 1) \right\} dx, \quad (5)$$

where \bar{x} is the x -coordinate of the centroid of the differential tower element dx , and l_s is the submerged length of the tower.

2.3. Total energies and equations of motion

Having arrived at the components of the kinetic and potential energies, we may simply sum the energies from the different sources to arrive at the total kinetic and potential energies. Adding Eqs. (2) and (3) gives the system kinetic energy

$$\mathbf{K}_E = \int_0^L \left\{ \frac{1}{8} \pi [\rho_T (D_o^2 - D_i^2) + C_{A\rho} D_o^2] y_t^2 + \frac{1}{128} \pi [\rho_T (D_o^2 - D_i^2) + C_{A\rho} D_o^2] \frac{y_{xt}^2 (D_o^2 - D_i^2)}{(1 + y_x^2)^2} \right\} dx. \quad (6)$$

Similarly, adding Eqs. (4) and (5) gives the system potential energy

$$\mathbf{P}_E = \int_0^L \left\{ \frac{1}{4} \pi \rho g D_o^2 (l_s - \bar{x}) (\sqrt{1 + y_x^2} - 1) + \frac{1}{128} \pi E (D_o^4 - D_i^4) \frac{y_{xx}^2}{(1 + y_x^2)^{3/2}} - \left[\frac{1}{4} \pi \rho_T (D_o^2 - D_i^2) (l - \bar{x}) + M \right] g (\sqrt{1 + y_x^2} - 1) \right\} dx. \quad (7)$$

We can now construct the Lagrangian. At this point, it is advantageous to reasonably assume small motions, meaning that the submerged length of the tower, l_s , is equal to the water depth, d , the centroid of the infinitesimal tower element, \bar{x} , is equal to the length coordinate x , and that $y_x \ll 1$. The Lagrangian becomes

$$\mathcal{L} = \int_0^L \left\{ \frac{1}{8} \pi (\rho_T + C_{A\rho}) (D_o^2 - D_i^2) \left(y_t^2 + \frac{(D_o^2 + D_i^2) y_{xt}^2}{16} \right) - \frac{1}{128} \pi E (D_o^4 - D_i^4) y_{xx}^2 + \frac{1}{8} \pi g y_x^2 [(D_o^2 - D_i^2) \rho_T (L - x) - D_o^2 \rho (d - x)] \right\} dx. \quad (8)$$

Note that the symbols used above are defined in Table 1. Next, we need to define the wave forces on the tower. Under the assumptions we have made, we can apply Morison's equation to find the drag and inertia forces on the tower:

$$Q_D = \frac{1}{2} C_D \pi \rho D |u_w - w_w y_x - y_t| [u_w - w_w y_x - y_t], \quad (9)$$

$$Q_M = \frac{1}{4} C_M \pi \rho D^2 (\dot{u}_w - \dot{w}_w y_x), \quad (10)$$

where w_w and u_w are the wave velocities in the x and y directions, respectively. These velocities can be expressed as [2]:

$$w_w = \frac{1}{2} H \omega e^{k(x-d)} \sin(ky - \omega t), \quad (11)$$

$$u_w = \frac{1}{2} H \omega e^{k(x-d)} \cos(ky - \omega t), \quad (12)$$

where H is the significant wave height, ω the wave frequency, and k is the wave number. The wave accelerations (\dot{w}_w, \dot{u}_w) are found by taking the time derivatives of the above expressions, leading to:

$$\dot{w}_w = -\frac{1}{2}H\omega(ky_t - \omega)e^{k(x-d)} \cos(ky - \omega t), \tag{13}$$

$$\dot{u}_w = \frac{1}{2}H\omega(ky_t - \omega)e^{k(x-d)} \sin(ky - \omega t). \tag{14}$$

There are two important points to note about the Morison forces. First, for our tower system, the generalized forces required by the Euler–Lagrange equations act in a direction opposite that of the Morison forces. Fig. 2 shows the direction of positive force used in the Euler–Lagrange equations. The Morison forces are positive in the direction of y opposite the direction in the figure, and therefore, the generalized force Q for the Euler–Lagrange equations may be written as $-(Q_D + Q_M)$.

Second, the definition of the Morison forces is in units of force per unit length. To apply these forces to our tower system, then, we need to integrate the above expressions for Q_D and Q_M along the length of the tower (with respect to x). This means that both sides of Eq. (1) involve an integral from 0 to L with respect to x , allowing us to find the equations of motion by operating on the integrand of each side.

We may now apply the Euler–Lagrange equations to the integrand of Eq. (8). For simplicity, we may rewrite Eq. (1) as $F_{\text{dyn}} = Q_D + Q_M$, meaning that F_{dyn} will be the negative of the result that comes out of the Euler–Lagrange equations, or

$$F_{\text{dyn}} = \frac{1}{64}\pi E(D_o^4 - D_i^4)y_{xxxx} + \frac{1}{4}\pi((D_o^2 - D_i^2)\rho_T + D_o^2 C_A \rho)y_{tt} - \frac{1}{64}\pi(D_o^4 - D_i^4)(\rho_T + C_A \rho)y_{xxt} - \frac{1}{4}\pi g\{[(D_o^2 - D_i^2)\rho_T(l - x) - D_o^2 \rho(d - x)]y_{xx} + y_x(D_o^2 \rho - (D_o^2 - D_i^2)\rho_T)\}. \tag{15}$$

At this point, we can include the internal damping force on the system. We assume this force is of the form $Q_{\text{dis}} = Cy_t$, where C is the internal damping coefficient. This dissipative force is subtracted from the right-hand side, giving the equation of motion $F_{\text{dyn}} = Q_D + Q_M - Q_{\text{dis}}$.

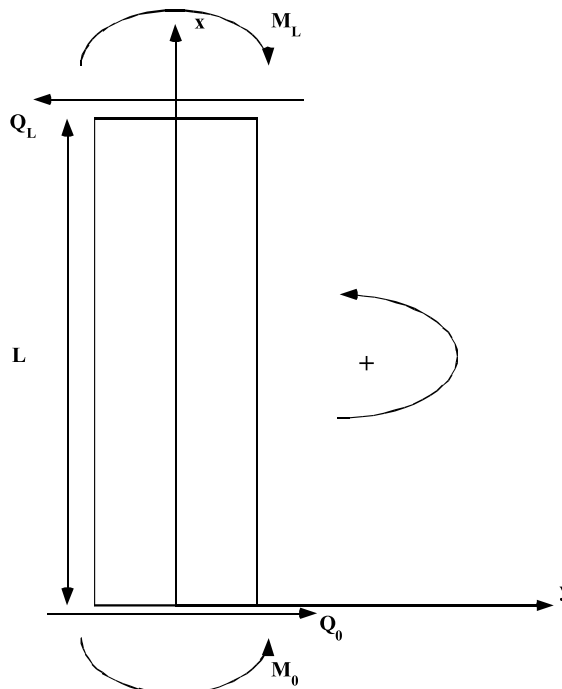


Fig. 2. Forces and moments on a tower element.

3. Numerical simulation

The resulting equation of motion ($F_{\text{dyn}} = Q_D + Q_M - Q_{\text{dis}}$) was simulated using MATLAB. In order to apply the finite difference method to find the spatial derivatives of the tower deflection (y_x, y_{xx}, y_{xxx}), we need to divide the tower into small segments. (A brief explanation of the finite difference method is given in Appendix A.) Since the error in the central difference operators that we use is proportional to the square of the length of these segments, we nondimensionalize the equation of motion. This way, the segment length is less than one, and the error in the operators is small. The nondimensionalizing factors that we use are L as a length scale, and $\sqrt{g/L}$ as a time scale. The nondimensional equation of motion is

$$\frac{1}{64} \pi \frac{D_o^4 - D_i^4}{D_o L^3} Y_{XXXX} - \frac{1}{4ED_o} \pi [(D_o^2 - D_i^2) \rho_T + D_o^2 C_A \rho] Y_{TT} - \frac{1}{4ED_o} \pi g \left\{ \left[(D_o^2 - D_i^2) \rho_T (1 - X) - D_o^2 \rho \left(\frac{d}{L} - X \right) \right] Y_{XX} + [D_o^2 \rho - (D_o^2 - D_i^2) \rho_T] Y_X \right\} + \frac{g}{64EL^2 D_o} \pi (D_o^4 - D_i^4) (\rho_T + C_A \rho) Y_{XXT} = \frac{Q_D + Q_M - Q_{\text{dis}}}{ED_o}. \tag{16}$$

The term multiplying Y_{XXT} is smaller than those multiplying Y_{TT} and Y_{XX} by a factor of L^2 ($\approx 122,000$) and is smaller than the term multiplying Y_{XXXX} by a factor of E/L ($\approx 6 \times 10^8$). This transverse moment of inertia term is ignored for the numerical study.

We apply a stochastic wave profile to the tower using the Pierson–Moskowitz energy spectrum as described by Chakrabarti [4]. The Pierson–Moskowitz power spectrum is translated into a time history via Borgman’s method [3]. A typical wave profile having significant wave height $H = 15$ m is pictured in Fig. 3. The response to such a profile is shown in Fig. 4, using the parameter values in Table 2, with material properties of steel. The initial conditions used are $Y(0) = 0.01$, $Y_T(0) = 0$. (These initial conditions are taken at $t = 0$ s, which corresponds to $T = 0$.)

Note that the response is stable; it varies slightly above the initial condition, then settles into a lower-amplitude steady-state oscillation in the presence of the stationary random forcing. The decay in the oscillation is mainly due to the damping in the Morison forcing, as the assumed structural dissipation is small. The response approaches zero due to the gravitational and buoyancy forces, as we shall see in more detail in the following section.

Another important consideration for the tower system is the maximum bending stress, since it is important that the material remain within the elastic range of behavior. The plot of the maximum bending stress versus time for the parameter set in Table 2 is given in Fig. 5. The maximum value in this plot is around 190 MPa, which is less than the yield stress of most types of steel. (As a specific example, the yield strength of AISI 4140 normalized steel is 655.0 MPa). There is no way to surmise a priori where along the tower length the maximum bending stress occurs, as

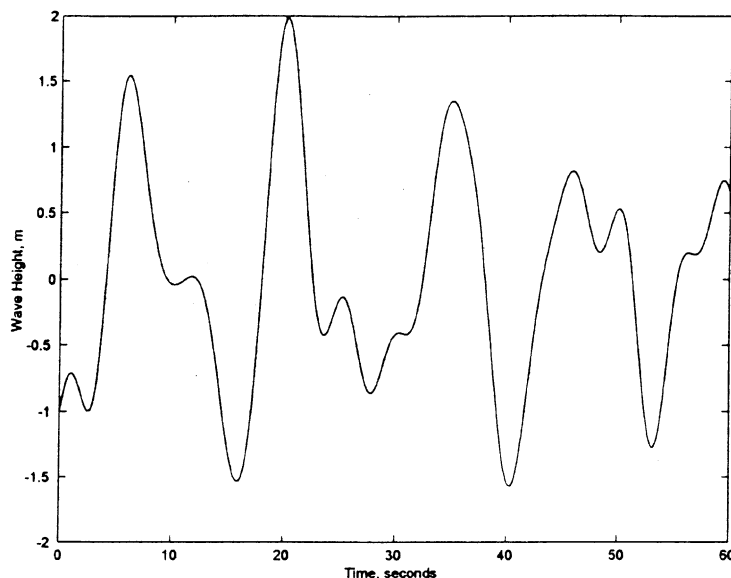


Fig. 3. Sample random wave height time history.

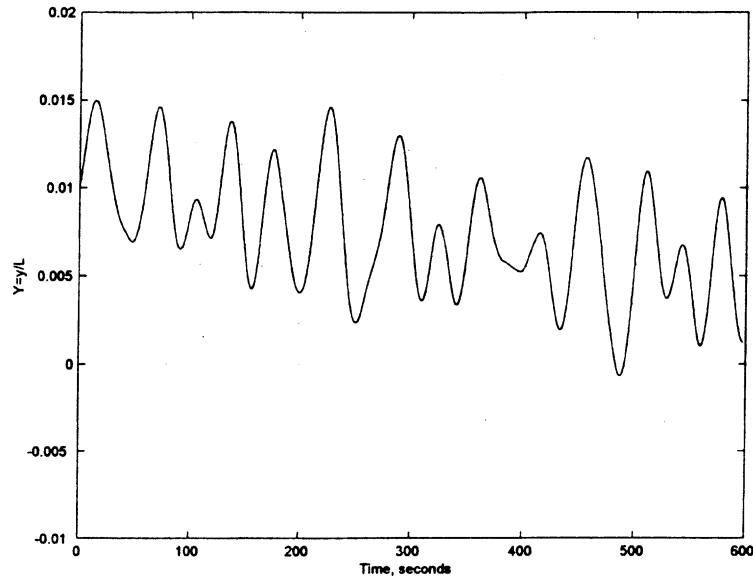


Fig. 4. Response of the tower to the parameter set in Table 2.

Table 2
Parameter values for numerical simulation

Quantity	Value
Tower length, L	350 m
Tower outer diameter, D_o	15 m
Tower inner diameter, D_i	14.8 m
Tower Young's modulus, E	207 GPa
Initial end displacement, Y	0.01
Mean water Level, d	350 m
Moment coefficient, C_M	1.5
Drag coefficient, C_D	0.75
Significant Wave Height, H	5 m
Internal damping coefficient, C	0.001

the boundary conditions at both ends correspond to zero moment. Thus, we make no statement concerning the point of application of the maximum bending stress; we only chart the maximum value.

4. Simplification of the model

We are interested to learn whether a simpler analytical model can capture the essential dynamic response, and therefore, we attempt to simplify the tower model. Looking at the nondimensional equations of motion, we find that the coefficients of the Y_X and Y_{XX} terms are small in comparison to that of the Y_{XXX} term. Specifically, referring to Eq. (16), the term multiplying Y_X and Y_{XX} is approximately of order $D_o/E \approx O(10^{-8})$. Conversely, the term multiplying Y_{XXX} is of order $D_o^3/L^3 \approx O(10^{-3})$. Removing terms due to Y_X and Y_{XX} effectively removes the potential energy due to gravity and buoyancy. At first glance, it seems that removing these terms should be unadvisable, since the classic articulated tower relies on the buoyancy force to keep it nearly vertical. However, the classic articulated tower also has a large buoyancy chamber on its end, that we have not modeled here. The response without these terms may provide us with some insight as to the behavior of the articulated tower minus the buoyancy chamber. We simulate the tower response, under identical parameters to those used above, to see what effect, if any, removal of these terms has on the numerical response. (For all MATLAB simulations, the same seed was given to MATLAB's random number generator, to allow for valid comparison between runs). The response is given in Fig. 6. Note that these responses are also for a tower with

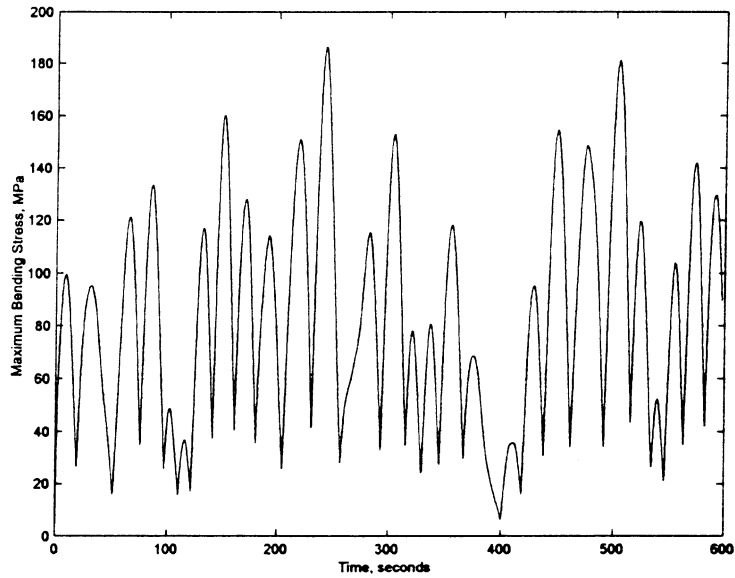


Fig. 5. Maximum bending stress corresponding to the parameter set in Table 2.

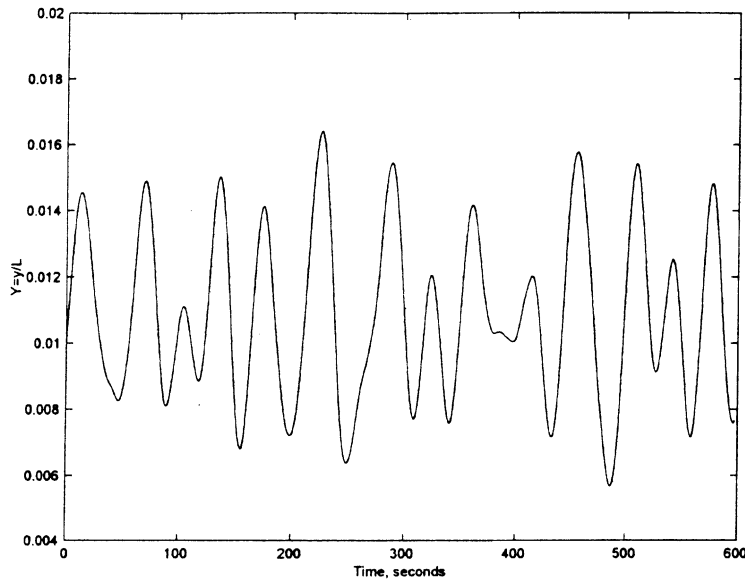


Fig. 6. Simulated response of the simplified system.

an inner diameter of 14.9 m. Though this configuration causes stresses exceeding the yield stress for steel, our purpose in this section is comparison between the responses when the Y_X and Y_{XX} terms are removed. While the system modeled here is not valid for practical purposes, it is quite valid for comparison purposes.

The plots in Figs. 4 and 6 have a similar shape. This would imply that the qualitative properties of the response are modelled by the Y_{XXX} term, and that the omitted Y_X and Y_{XX} terms are responsible only for changing the midpoint of the response oscillation toward zero. To better show this, the full and simplified responses are plotted on the same axes in Fig. 7.

Again, the shapes of the responses are identical; the main difference is that while the simplified model oscillates around the initial condition, the full model experiences a decaying oscillation. The reason for this difference becomes

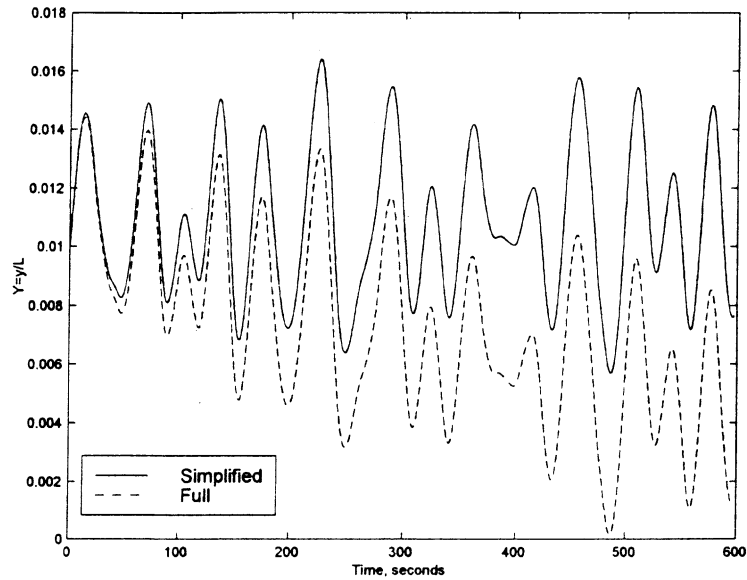


Fig. 7. Response of both the full and simplified models.

clear when we examine the physical significance of the terms removed. These terms contain the gravity and buoyancy forces on the tower system. In particular, the buoyancy force, although conservative, opposes the tower deflection since its magnitude increases with the motion of the tower; as the tower becomes more submerged it displaces more water and a greater upward force results. The net effect of the tower buoyancy force, then, is to place the equilibrium point of the tower motion at zero deflection, since, in the absence of wave and current forces, the tower will experience zero lateral force at zero deflection.

To better understand what physical information was being removed from the system, we simulated both models with zero wave forcing. The response of the full model is given in Fig. 8. We see from the figure that the tower end slowly approaches zero displacement from its initial location of 0.01 (nondimensional). The simplified model had no motion (i.e., the response plot was a horizontal line passing through the initial condition), which we expect from the equation of

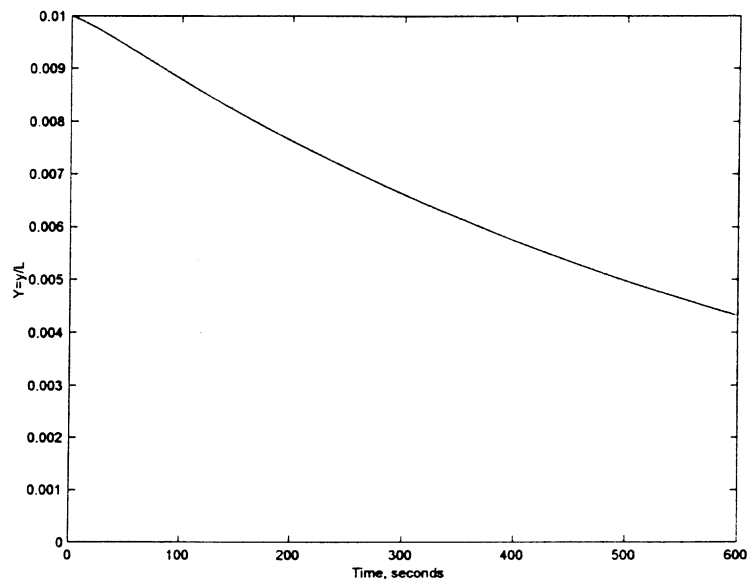


Fig. 8. Response of the full model to zero wave forces.

motion. (Our initial conditions include no bending, only a rigid-body displacement, so the fourth derivative of the displacement is zero.) This free vibration comparison illustrates the tendency of the gravitational and buoyancy forces to return the tower to a vertical position.

The simplified model gives us some useful information, however. First, it faithfully models the shape of the response curve, again implying that the Y_{xxxx} term is responsible for the profile of the response, in combination with the wave forcing. Additionally, it provides us with an upper bound on the motion of the tower system, which may be useful for some types of failure analysis. For our purposes, however, the minimal gain in computational time is not worth the loss of the gravity and buoyancy information caused by this model.

5. Parametric study

A logical step in this work is to examine the response of the tower under different environmental loads. For this paper, we accomplish this by changing the characteristics of the wave profile, which is best done by changing the significant wave height. Also, the response of towers made of different materials, say, aluminum, would be appropriate to examine. Another interesting study would be to look at the difference caused by changing the inner diameter of the tower (making it more or less solid than the tower above). Our basis for comparison is the above simulation for a steel tower having inner diameter 14.8 m and subjected to a wave profile with significant wave height $H = 5$ m, the results of which are given in Fig. 4.

In Fig. 9, we have the response of the tower to a wave profile having $H = 15$ m. This case shows several differences from the response to the original parameter set. First, the maximum deflection increases from 0.015 (5.25 m) to approximately 0.02 (7.00 m). In the allotted time frame of 10 min, the tower end passes through the zero position, whereas in the response to the original set of parameters, the tower motion approached but did not cross zero. Also, the general shape of the response has completely changed, with the introduction of smaller oscillations (high-frequency content) in between the larger-scale motion. Thus, changing the significant wave height has had a profound effect on the system response. The presence of the high-frequency oscillations in the response can also shorten the expected fatigue life of the structure.

We also look at the maximum bending stress for this case, plotted in Fig. 10. The maximum over the course of the simulation is about 450 MPa. This stress is less than the yield stress of many types of steel, so the tower can be designed to withstand strong sea conditions using an inner diameter of 14.8 m.

To further illustrate the effect of significant wave height on tower response, we examine the behavior of the same tower with $H = 25$ in Fig. 11. Here, the general shape of the response is more similar to that of the response to $H =$

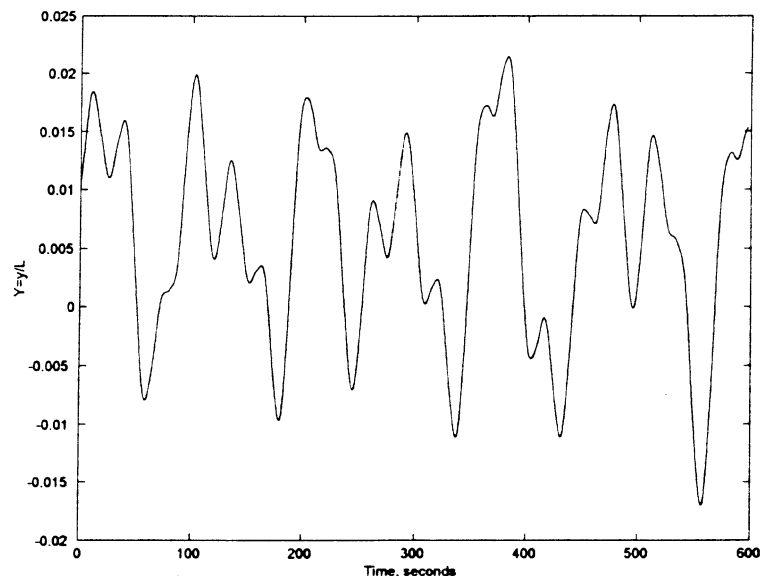


Fig. 9. Response to significant wave height $H = 15$ m.

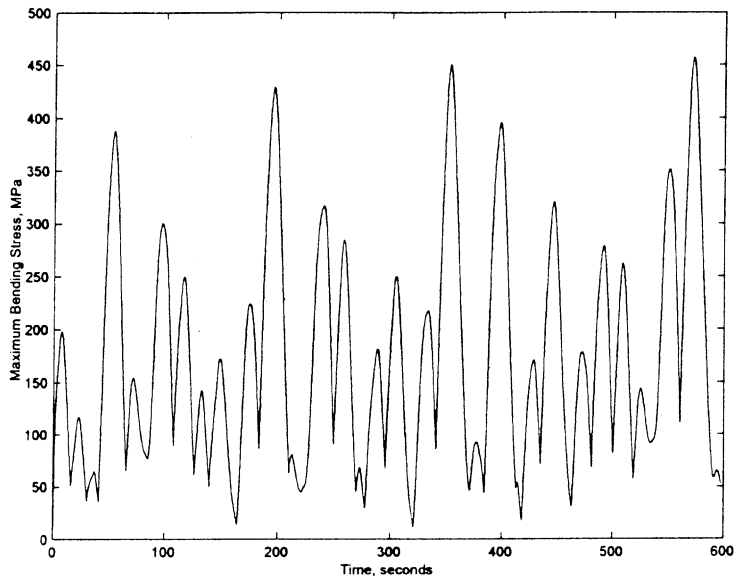


Fig. 10. Maximum bending stress for $H = 15$ m.

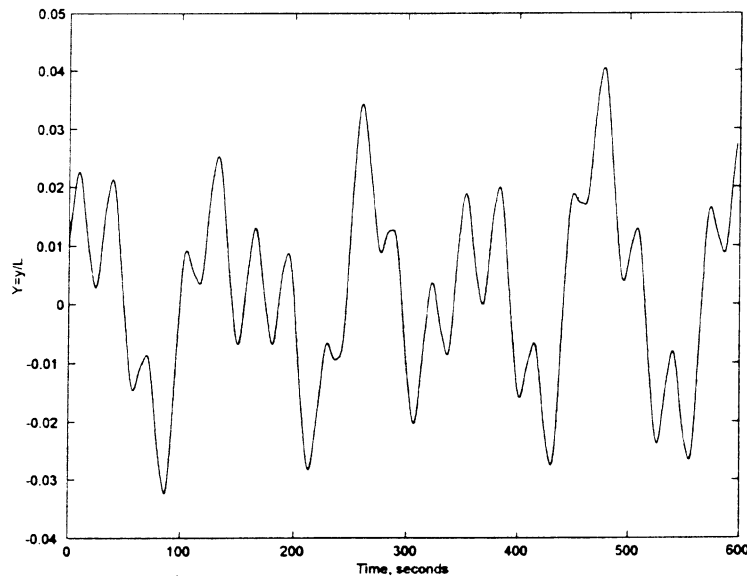


Fig. 11. Response of the steel tower to $H = 25$ m.

15 m, as we might expect, since $H = 15$ m and $H = 25$ m both represent extreme ocean conditions. The maximum response magnitude has again shifted, up to a little over 0.040 (14.0 m), and we see more of an oscillation about the neutral position $Y = 0$. Changing the wave profile has a strong effect on the response, as we would expect, since the wave profile dictates the forcing experienced by the system.

Since the maximum displacement has almost doubled, we expect an increase in the maximum bending stress for this case, plotted in Fig. 12. The maximum over the course of the simulation time is about 750 MPa, which exceeds the yield strength of most types of steel. This introduces a design safety parameter to the tower system; if the tower is to be placed in an area where very strong sea conditions are likely, the inner diameter of 14.8 m is unacceptable.

Next, we give the response of an aluminum tower ($E = 72$ GPa) to the wave profile with $H = 5$ m in Fig. 13. The main difference between this response and that of the steel tower to an identical wave load, as may be expected, is that

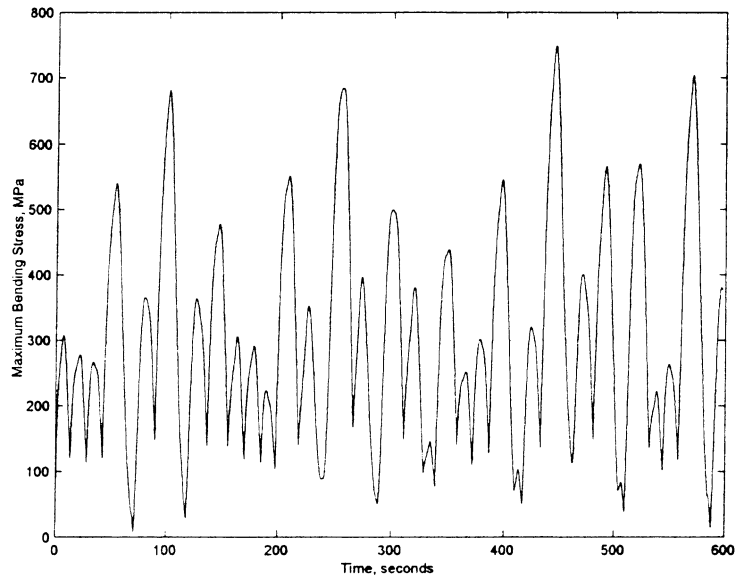


Fig. 12. Maximum bending stress for the case $H = 25$ m.

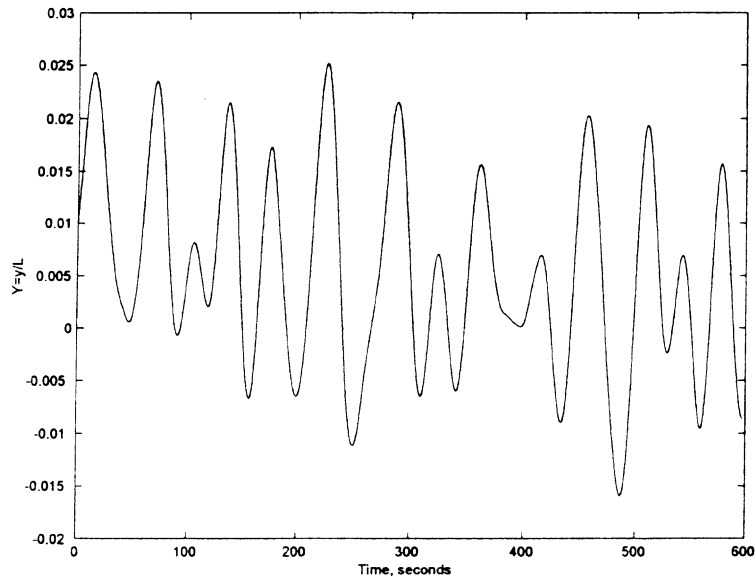


Fig. 13. Response of an aluminum tower to the parameters given in Table 2.

the aluminum tower experiences a higher-magnitude deflection than the steel tower. The maximum deflection of the steel tower was about 0.015 (5.25 m), whereas the maximum deflection for the aluminum tower is about 0.025 (8.75 m). The valleys of the oscillation over the 10-min span given is also different. The steel tower deflection never crosses zero, where the aluminum tower deflection goes as low as -0.015 (-5.25 m). It seems that the material used has an important effect on the magnitude of response of the tower. But the response is still stable and appears to have settled into an oscillation about zero in a manner similar to the steel tower. This shows that the buoyancy force still has a strong centering effect on this configuration.

As we would expect, the increase in end displacement also leads to an increase in the maximum bending stress, plotted in Fig. 14. The maximum bending stress here is about 170 MPa, which is within the elastic range for some types

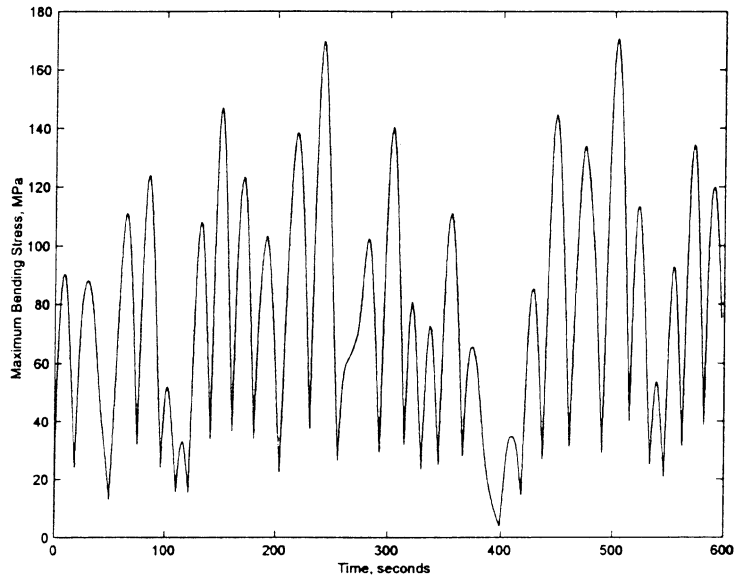


Fig. 14. Maximum bending stress for the aluminum tower, $H = 5$ m.

of aluminum (e.g., 2024-T4). So, an aluminum tower is feasible for calmer sea conditions, if a larger displacement than the steel tower is acceptable.

If we increase the significant wave height to $H = 15$ m, we get the response pictured in Fig. 15. The differences between this response curve and that in Fig. 13 are similar to those between Figs. 4 and 9. That is, the response to the larger significant wave height has a greater maximum magnitude and more oscillations through zero than the response to the smaller wave height. Comparing Fig. 15 to Fig. 9, we see again that the aluminum tower response has a greater maximum magnitude than the steel tower. But, note also that the shape of the response is generally the same for the steel and aluminum towers, implying that the overall form of the response is independent of the material used.

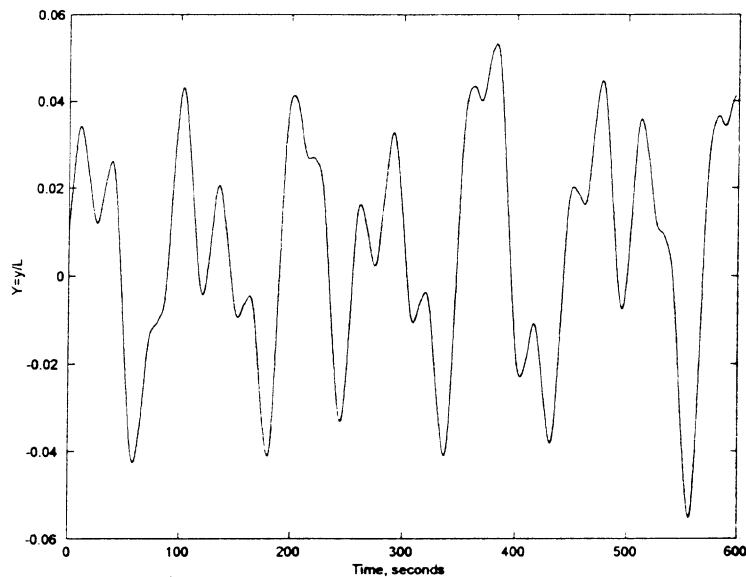


Fig. 15. Response of the aluminum tower to $H = 15$ m.

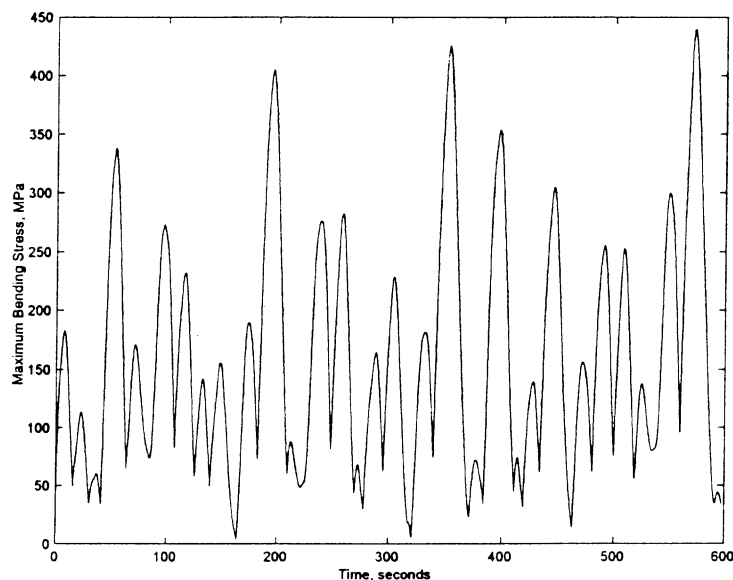


Fig. 16. Maximum bending stress for the aluminum tower, $H = 15$ m.

We again expect the increase in tower deflection to correspond to an increase in the bending stress, pictured in Fig. 16. The maximum value here is 450 MPa, which exceeds the yield stress of almost all types of aluminum. This shows the inferiority of aluminum as a tower material, since an aluminum tower can only withstand a relatively narrow range of sea conditions without plastic deformation. Thus, we do not examine the aluminum tower response to $H = 25$ m, as we know it will undergo plastic deformation in this case.

The third type of tower examined in this study is again made of steel, but the cross-sectional characteristics of the tower are changed. The tower for the next three parameter simulations have $D_o = 15$ m, as for all the previous studies, but the inner diameter is decreased from $D_i = 14.8$ m to $D_i = 14.5$ m. The response to a wave profile having $H = 5$ m is plotted in Fig. 17. The maximum deflection of the tower is actually increased, to slightly over 0.015 (5.25 m), where the

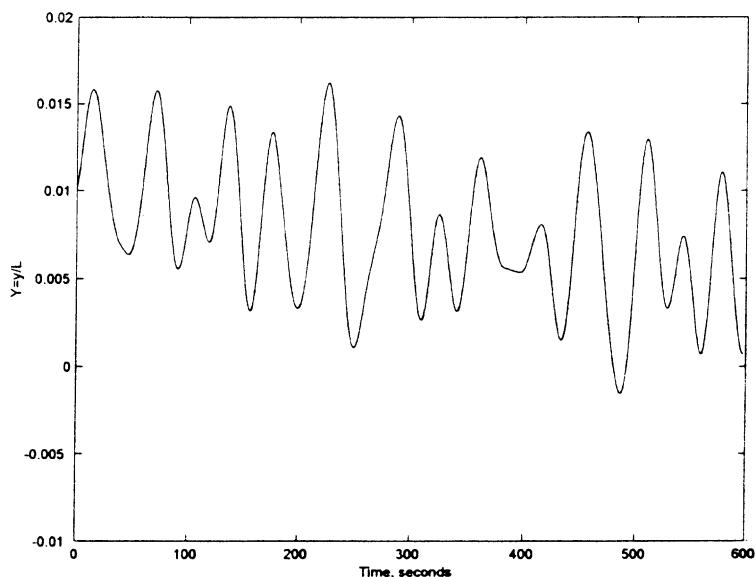


Fig. 17. Response of the thicker steel tower to $H = 5$ m.

original tower had a maximum deflection of 0.015. The response of the thicker tower drops to below zero within the given time span, where the original tower response does not. The shape of the response is similar to that of the original tower, and both responses seem to be tending toward zero.

The plot of the maximum bending stress shows that this larger displacement does not correspond to larger bending stress (see Fig. 18). The maximum bending stress is about 120 MPa, compared to 190 MPa for the steel tower with $D_i = 14.8$ m. An increase in the inner diameter seems to lead to smaller bending stresses.

Next, we look at the response when the significant wave height is increased to 15 m. The simulated response is given in Fig. 19. As with the original tower, the maximum deflection increases with the larger significant wave height. In comparison to the response of the original tower to significant wave height $H = 15$ m, we see that the maximum de-

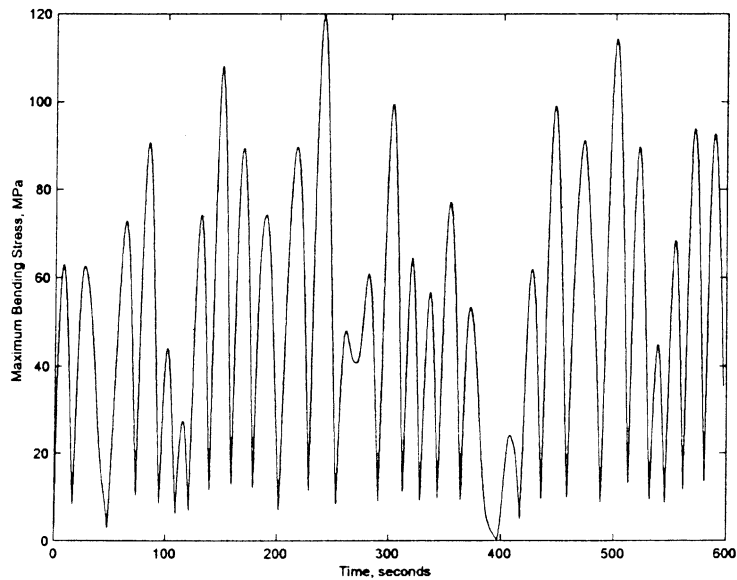


Fig. 18. Maximum bending stress for a steel tower, $D_i = 14.5$ m, $H = 5$ m.

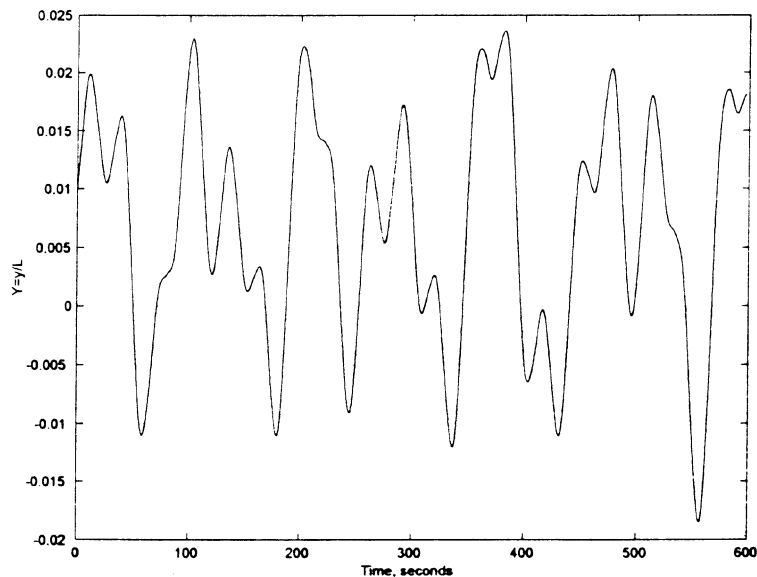


Fig. 19. Response of the steel tower with $D_i = 14.5$ m to $H = 15$ m.

flection is again larger for the tower with $D_i = 14.5$ m. Some of the qualitative aspects of the response are similar for both towers, but now we begin to see some differences, like the behavior around $t = 200$ s and $t = 375$ s. Changing the cross-sectional properties of the tower has changed the nature of the response more than changing the material properties.

As we saw in the maximum bending stress plot for $H = 5$ m, the thicker tower experiences a smaller stress. The maximum bending stress shown in Fig. 20 is about 300 MPa, which is 33% lower than the maximum stress for the tower with $D_i = 14.8$ m and the same sea conditions.

Fig. 21 gives the response of this tower to a wave profile having significant wave height $H = 25$ m. Again, the maximum response of the tower with $D_i = 14.5$ m is greater than that of the tower having $D_i = 14.9$ m, by about

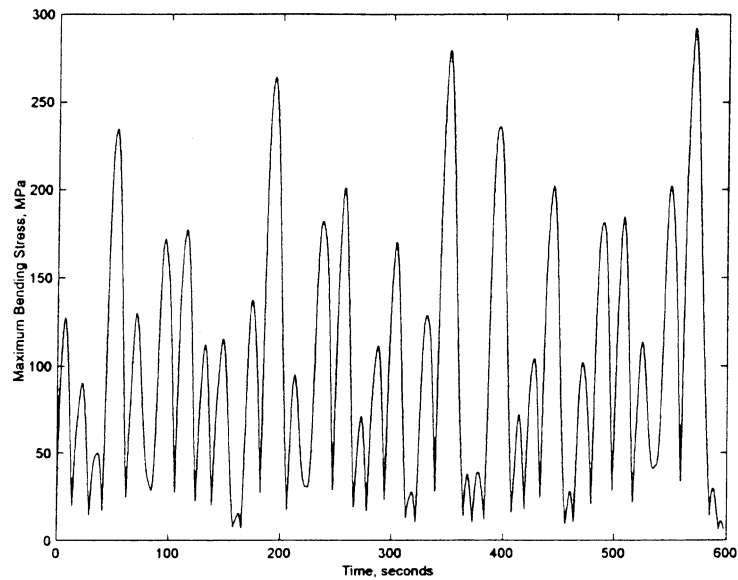


Fig. 20. Maximum bending stress for the thicker steel tower, $H = 15$ m.

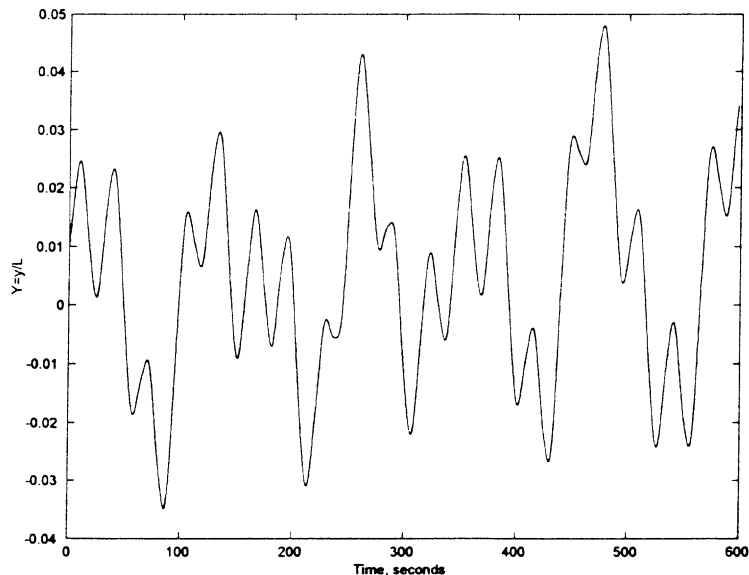


Fig. 21. Response of the steel tower having $D_i = 14.5$ m to $H = 25$ m.

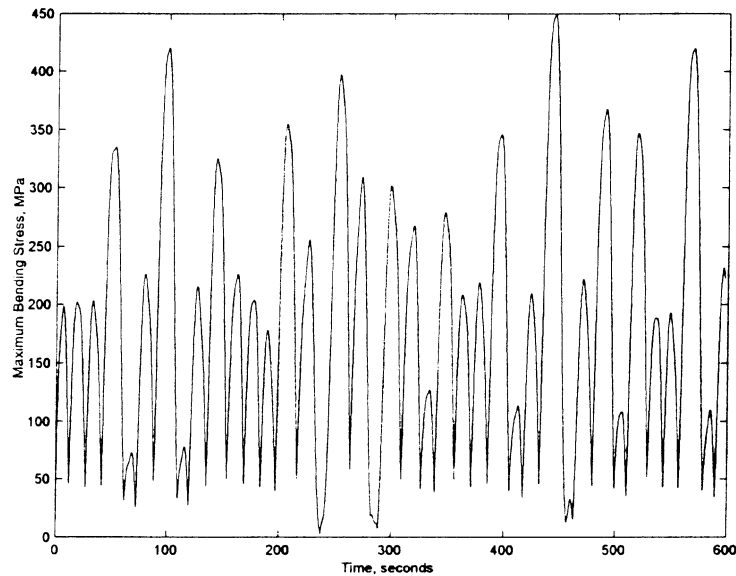


Fig. 22. Maximum bending stress for a steel tower, $D_i = 14.5$ m, $H = 25$ m.

0.05 (17.5 m) to 0.03 (10.5 m). The form of the response is once more similar for both the original and thicker-walled tower.

Finally, Fig. 22 shows that the maximum bending stress for this case is less than that for the tower having $D_i = 14.8$ m to the same sea conditions. Here, the maximum bending stress is about 450 MPa, well below the yield point of many types of steel and 40% lower than the maximum stress experienced by the tower with $D_i = 14.8$ m.

The increased response magnitude of the tower with $D_i = 14.5$ m seen for all three tested wave profiles merits further discussion. Intuitively, we may think that the thicker tower should experience less deflection, either because of the increased moment of inertia or because of the increased mass of the tower. In order to understand why the thicker tower should deflect more, we need to look at the forces acting on the tower: gravity, buoyancy, and the Morison wave forces. The Morison inertia force is oscillatory in nature, and does not consistently oppose nor aid the tower deflection. The only external forces that oppose the tower motion are the Morison drag force and the buoyancy force (the internal damping force also opposes the motion, but is small relative to the external forces). The drag force is dependent upon the surface area of the tower, which is unchanged; thus, the Morison drag force remains approximately equal for the thicker tower. The buoyancy force is also unchanged, since the buoyancy force is dependent on the density of water and the volume of the tower, both of which are constant. However, the density of a steel tower having $D_o = 15$ m, $D_i = 14.5$ m and $L = 350$ m is 505.9 kg/m^3 , where the density if we increase D_i to 14.8 m is 204.0 kg/m^3 . (Note that we assume the hollow portion of the tower to be filled with air.) This means that the gravitational force acting on the thicker tower is about 2.5 times that acting on the original tower. Since the gravitational force tends to pull the tower down toward the water surface, we would expect an increased deflection for the more massive tower.

Most importantly, we see that the responses for all parameter sets are bounded. This implies that the tower system is stable to the limit of the parameters tested here. Also, we have seen that the tower can be designed to avoid plastic deformation for the environmental loads tested.

6. Conclusions

A nonlinear, continuous model for a flexible ocean tower has been derived using Hamilton's Principle. The tower motion has been demonstrated as stable under Morison wave forces, gravity, and buoyancy. An attempted simplification of the model has been presented, and shows usefulness for finding the qualitative behavior of the system and for a maximum deflection analysis.

A parameter study performed using the tower model derived here has shown the following:

- The maximum deflection of the tower increases with increasing significant wave height, H .
- The material used in constructing the tower has an effect on the maximum deflection of the tower.

- The material used has no effect on the qualitative aspects of the tower response.
- Increasing the inner diameter of a hollow tower causes an increase in maximum tower deflection, due to the increased mass of the tower.
- Increasing the inner diameter of the tower has a small effect on the qualitative aspects of the response.
- Increasing the inner diameter of the tower decreases the maximum bending stress experienced by the tower.
- The tower motion is stable for all parameter sets tested.

Acknowledgements

This work is supported by the Office of Naval Research Grant No. N00014-97-1-0017. The authors are grateful for this support from ONR and program manager Dr. Thomas Swean as well as for his interest in our work.

Appendix A. The finite difference method

A.1. Central difference operators

In order to simulate the equations of motion for the tower system, we apply the finite difference method to represent the spatial derivatives of the tower deflection. The length of the tower is divided into N parts, as shown in Fig. 23, giving us N nonlinear coupled ordinary differential equations, which we integrate using MATLAB. We use central difference operators for the entire length, meaning that we need to introduce dummy nodes at the top and bottom end of the tower. These dummy nodes introduce certain constraints for the nodes at either end of the tower. The error of this approximation is of the order $O[h^2]$, where h is the spacing between nodes,

$$h = \frac{L}{N}. \quad (\text{A.1})$$

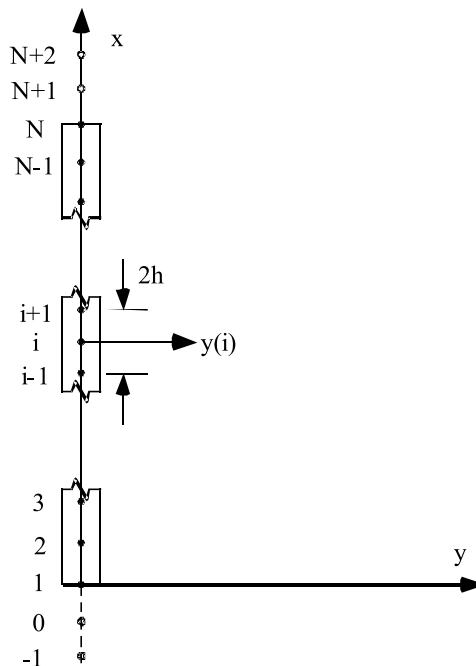


Fig. 23. Discretization of the Tower.

Referring to [2], the central difference operators are:

$$\begin{aligned}
 y_x(i) &= \frac{y(i+1) - y(i-1)}{2h}, \\
 y_{xx}(i) &= \frac{y(i+1) - 2y(i) + y(i-1)}{h^2}, \\
 y_{xxx}(i) &= \frac{y(i+2) - 2y(i+1) + 2y(i-1) - y(i-2)}{2h^3}, \\
 y_{xxxx}(i) &= \frac{y(i+2) - 4y(i+1) + 6y(i) - 4y(i-1) + y(i-2)}{h^4}, \\
 y_{xt}(i) &= \frac{y_t(i+1) - y_t(i-1)}{2h}, \\
 y_{xtt}(i) &= \frac{y_{tt}(i+1) - y_{tt}(i-1)}{2h}, \\
 y_{xttt}(i) &= \frac{y_{tt}(i+1) - 2y_{tt}(i) + y_{tt}(i-1)}{h^2}.
 \end{aligned} \tag{A.2}$$

The subscript notation used above for derivatives of y is the same as in the main paper. Applying these operators is straightforward for $i = 3, 4, \dots, N-2$, as all the necessary quantities for the finite difference scheme are real nodes. In order to get operators for $i = 1, 2, N-1, N$, we need to apply constraints that are implied by the end conditions.

A.2. Lower end

At the lower end, we assume that the tower is pinned, giving the boundary conditions:

$$\begin{aligned}
 y(0, t) &= 0, \\
 y_{xx}(0, t) &= 0.
 \end{aligned} \tag{A.3}$$

That is, the tower experiences neither transverse deflection nor moment at its bottom. The first condition implies $y(1) = 0$. The equation for the moment at the first node is

$$y_{xx}(1) = \frac{y(2) - y(1) + y(0)}{h^2} = 0, \tag{A.4}$$

which leads a constraint on the displacement of dummy node 0:

$$y(0) = -y(2). \tag{A.5}$$

The pinned boundary condition also means that we do not need to find the displacement of dummy node -1 , which appears in the equation for $y_{xxxx}(1)$, because we do not need to solve the differential equation for the displacement of node 1; it is given by the boundary condition.

A.3. Upper end

The boundary conditions at the top of the tower are considerably more complex than those at the bottom. We assume a free end at the top of the tower, which therefore cannot support moment nor shear. The resulting boundary conditions are:

$$\begin{aligned}
 y_{xx}(N) &= 0, \\
 y_{xxx}(N) &= 0.
 \end{aligned} \tag{A.6}$$

Applying the equation for the moment at node N , we see that

$$y_{xx}(N) = \frac{y(N+1) - 2y(N) + y(N-1)}{h^2} = 0 \tag{A.7}$$

or, solving for $y(N+1)$ in terms of the real displacements $y(N)$ and $y(N-1)$:

$$y(N+1) = 2y(N) - y(N-1). \tag{A.8}$$

Next, we look at the equation for the shear at node N

$$y_{xxx}(N) = \frac{y(N+2) - 2y(N+1) + 2y(N-1) - y(N-2)}{h^2} = 0. \quad (\text{A.9})$$

We can solve Eq. (A.9) for $y(N+2)$, arriving at

$$y(N+2) = 2y(N+1) - 2y(N-1) + y(N-2) \quad (\text{A.10})$$

or, purely in terms of real node displacements,

$$y(N+2) = 4y(N) - 4y(N-1) + y(N-2). \quad (\text{A.11})$$

Having expressions for the displacements of the dummy nodes, we have all the information needed to solve the finite difference equations.

A.4. Numerical application

We can apply the central difference operators in Eq. (A.2) to transform our differential equation for $y(x, t)$ into N second-order coupled ordinary differential equations. This system of equations is then coded into a MATLAB script file, and solved numerically. As noted above, the central difference operators have error of order $O[h^2]$. If we introduce nondimensional lengths, as noted in the body of the paper, our spacing between nodes becomes $h = 1/N$, with an error of $1/N^2$. The simulations in the paper use 20 nodes, so the error is of the order of $1/400$, or about 0.0025.

References

- [1] Adrezn R, Bar-Avi P, Benaroya H. Dynamic response of compliant offshore structures – review. *J Aerospace Eng* 1996;9(4):114–31.
- [2] Bar-Avi P, Benaroya H. *Nonlinear dynamics of complaint offshore structures*. Lisse, The Netherlands: Sweets and Zeitlinger Publishers; 1997.
- [3] Borgman L. Ocean wave simulation for engineering design. *J Waterways Div* 1969;95(WW4):557–83.
- [4] Chakrabarti S. *Hydrodynamics of offshore structures*. Southampton, UK: Computational Mechanics Publications; 1987.
- [5] Lanczos C. *The variational principles of mechanics*. New York: Dover Publications; 1986.